Katariina A. H. Myller[1]
Department of Applied Physics,
University of Eastern Finland,
P.O. Box 1627,
Kuopio FI-70211, Finland;
Diagnostic Imaging Center,
Kuopio University Hospital,
P.O. Box 100,
Kuopio FI-70029, Finland
e-mail: katariina.myller@uef.fi

Rami K. Korhonen
Department of Applied Physics,
University of Eastern Finland,
P.O. Box 1627,
Kuopio FI-70211, Finland
e-mail: rami.korhonen@uef.fi

Juha Töyräs
Department of Applied Physics,
University of Eastern Finland,
P.O. Box 1627,
Kuopio FI-70211, Finland;
Diagnostic Imaging Center,
Kuopio University Hospital,
P.O. Box 100,
Kuopio FI-70029, Finland;
School of Information Technology and
Electrical Engineering,
The University of Queensland,
St Lucia Qld, Brisbane 4072, Australia
e-mail: juha.toyras@uef.fi

Petri Tanska
Department of Applied Physics,
University of Eastern Finland,
P.O. Box 1627,
Kuopio FI-70211, Finland
e-mail: petri.tanska@uef.fi

Sami P. Väänänen
Department of Applied Physics,
University of Eastern Finland,
P.O. Box 1627,
Kuopio FI-70211, Finland;
Diagnostic Imaging Center,
Kuopio University Hospital,
P.O. Box 100,
Kuopio FI-70029, Finland;
Central Finland Central Hospital,
Department of Physics,
Keskussairaalantie 19,
Jyväskylä FI-40620, Finland
e-mail: sami.vaananen@uef.fi

Jukka S. Jurvelin
Department of Applied Physics,
University of Eastern Finland,
P.O. Box 1627,
Kuopio FI-70211, Finland
e-mail: jukka.jurvelin@uef.fi

Clinical Contrast-Enhanced Computed Tomography With Semi-Automatic Segmentation Provides Feasible Input for Computational Models of the Knee Joint

Computational models can provide information on joint function and risk of tissue failure related to progression of osteoarthritis (OA). Currently, the joint geometries utilized in modeling are primarily obtained via manual segmentation, which is time-consuming and hence impractical for direct clinical application. The aim of this study was to evaluate the applicability of a previously developed semi-automatic method for segmenting tibial and femoral cartilage to serve as input geometry for finite element (FE) models. Knee joints from seven volunteers were first imaged using a clinical computed tomography (CT) with contrast enhancement and then segmented with semi-automatic and manual methods. In both segmentations, knee joint models with fibril-reinforced poroviscoelastic (FRPVE) properties were generated and the mechanical responses of articular cartilage were computed during physiologically relevant loading. The mean differences in the absolute values of maximum principal stress, maximum principal strain, and fibril strain between the models generated from semi-automatic and manual segmentations were <1 MPa, <0.72% and <0.40%, respectively. Furthermore, contact areas, contact forces, average pore pressures, and average maximum principal strains were not statistically different between the models ($p > 0.05$). This semi-automatic method speeded up the segmentation process by over 90% and there were only negligible differences in the results provided by the models utilizing either manual or semi-automatic segmentations. Thus, the presented CT imaging-based segmentation method represents a novel tool for application in FE modeling in the clinic when a physician needs to evaluate knee joint function.
[DOI: 10.1115/1.4045279]

[1]Corresponding author.
Manuscript received December 21, 2018; final manuscript received October 22, 2019; published online January 17, 2020. Assoc. Editor: Anton E. Bowden.

Simo Saarakkala
Department of Diagnostic Radiology,
Oulu University Hospital,
Kajaanintie 50,
Oulu FI-90220, Finland;
Research Unit of Medical Imaging,
Physics and Technology,
University of Oulu,
P.O. Box 5000,
Oulu FI-90014, Finland
e-mail: simo.saarakkala@oulu.fi

Mika E. Mononen
Department of Applied Physics,
University of Eastern Finland,
P.O. Box 1627,
Kuopio FI-70211, Finland
e-mail: mika.mononen@uef.fi

Introduction

Osteoarthritis (OA) is a common joint disease; the prevalence of knee OA has been estimated to be 3.8% of the world population [1], burdening the lives of over 260 million people. This painful and immobilizing joint disease may be initiated and worsened by abnormal joint loading, i.e., high impact loads [2] or repetitive joint loads generated during daily physical activities such as walking or running [3,4]. Unfortunately, the routine diagnostics of OA has mostly focused on the evaluation of symptoms or anatomic features, such as chronic pain or the decrease in joint space width, which are more characteristic of later stages of the disease. Therefore, if we wish to prevent the progression of the disease or to predict its onset, it would be advantageous to have more sophisticated imaging and diagnostic methods.

Biomechanical modeling can be used for the evaluation of joint mechanics under physiologically relevant loading conditions [5,6], providing diagnostically valuable information on the function of the joint in terms of tissue stresses and strains. Computational finite element (FE) models enable simulation of strains in the collagen fibrils and assessing progression of damage; these models have also been used to estimate cell death and changes in tissue structure around cartilage lesions as well as to predict the progression of OA [7–15]. Biomechanical analysis techniques are also relevant for the investigation of other normal and altered states in a knee joint, not only for investigation of cartilage damage and OA [16,17].

A major obstacle to the clinical application of modeling approaches and the quantitative analysis of knee joint tissues is that they demand information on subject-specific joint geometries. In most cases, the knee joint geometry for computational modeling is obtained via manual segmentation of the joint structures [18], which is a very time-consuming task to perform for each individual subject. Sophisticated techniques, such as statistical shape modeling and neural networks, have been exploited in the development of automatic segmentation methods [19–23]. These methods have proven to be superior to less complex techniques, for instance, those based on simple thresholding. Several automatic and semi-automatic segmentation methods have been introduced for segmentation of knee joint connective tissues from magnetic resonance and computed tomography (CT) images [20,22–25]. However, the feasibility of these methods has not typically been tested in computational modeling, possibly due to the laborious work required in transferring the generated segmentations into computationally sufficient and compatible forms.

Previously, a semi-automatic method was developed to segment contrast-enhanced CT images [25]. In contrast-enhanced CT imaging, contrast agent is administered into the joint space, enabling visualization of articular cartilage [26,27]. The previous method was designed to segment healthy and degenerated cartilage from contrast-enhanced CT images of knee joints. The method was based on cortical bone determination and subsequent automatic segmentation of articular cartilage. It was shown that semi-automatic segmentations of articular cartilage were reproducible and accurate as compared with manual segmentations. However, the applicability of this method to provide useful geometries for computational FE modeling of the knee joint has not yet been evaluated. This would be important as automated segmentation of joint tissues from clinical images and FE modeling of joint biomechanics would ideally enable clinical diagnostics of joint function to predict the onset and progression of OA.

This study aims to investigate the suitability of a recently developed semi-automatic segmentation method for contrast-enhanced CT images [25] in biomechanical FE modeling of knee joint function. Manually generated segmentations were used for comparison. FE model predictions were compared between the models generated by manual and semi-automatic segmentation methods during physiologically relevant loading. We hypothesize that the FE models generated based on the semi-automatic segmentation method would yield similar values for cartilage stresses and strains as the FE models generated based on manual segmentation.

Methods

Imaging and Segmentation. In this study, both manual and semi-automatic segmentations of femoral and tibial cartilages were used. The segmentations were based on the contrast-enhanced CT data (105 mM, Hexabrix^{TM} 320, Guerbet, Roissy, France; diluted to 0.9% saline for intra-articular injection) from seven patients (Age = 57.7±5.1 years, BMI = 27.9±4.9 kg/m^2) with persistent knee pain and arthroscopically confirmed cartilage degeneration. The knees had International Cartilage Repair Society (ICRS) scored lesions (grades 1–3) evaluated by an experienced orthopedic surgeon. The subjects provided written informed consent, and the study protocol was approved by the Ethical Committee of the Northern Ostrobothnia Hospital District (Decision No. 33/2010). Moreover, the study adhered to the Declaration of Helsinki.

The proximal tibia and distal femur bones were segmented from the CT images by drawing axial contours sparsely using Stradwin (v5.2, Department of Engineering, University of Cambridge, UK). 3D surfaces were generated from these contours.

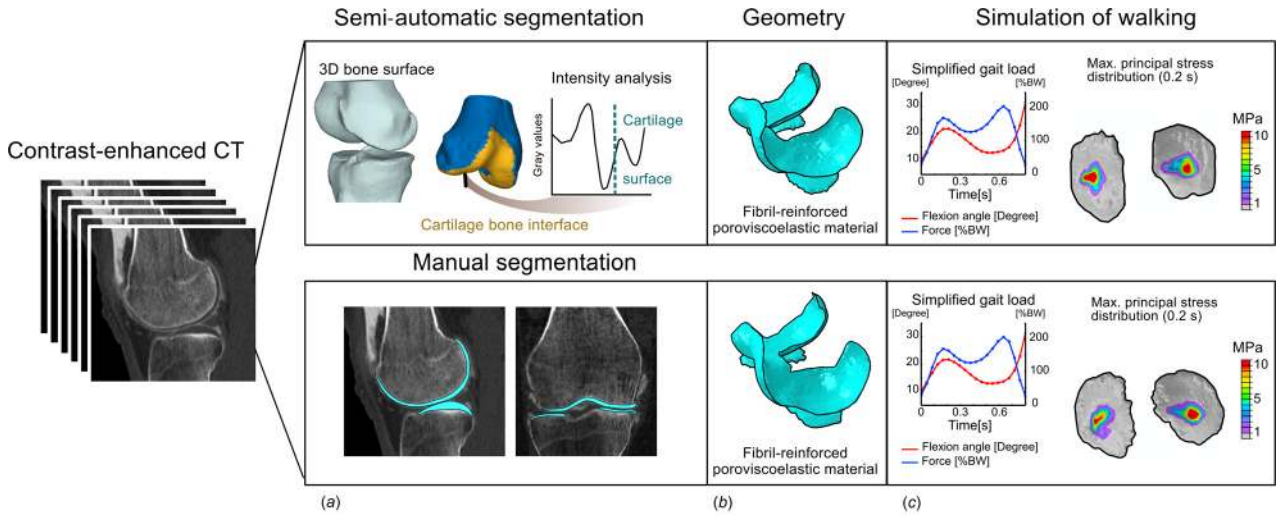

Fig. 1 The workflow of the study: (*a*) The cartilages were segmented using both semi-automatic [25] and manual methods, (*b*) fibril-reinforced poroviscoelastic (FRPVE) material properties were implemented in the geometries of the articular cartilage, (*c*) FE modeling was conducted applying physiologically relevant loading from the literature [32,33]. Computational results, such as maximum principal stresses and strains, were compared between the methods. Additionally, the surfaces of semi-automatic segmentations were postprocessed similarly as conducted in the manual segmentations. To analyze the effect of postprocessing, the models generated from "modified semi-automatic" segmentations were also compared with the models generated from manual and semi-automatic segmentations.

Subsequently, cortical bone thickness and periosteal and endocortical surfaces, i.e., outer and inner cortical surfaces, were determined. The optimization method utilizes deconvolution of intensity profiles perpendicular to cortical surface. The algorithm captures both periosteal and endocortical surfaces simultaneously. This was done because optimization of cortical thickness is required when bone–cartilage interface is obtained accurately [28]. Regions where cartilage covers bone epiphyses were determined by registering bone surface templates, which included the bone-cartilage region information, on the generated periosteal surfaces of femur and tibia (Matlab, R2015a, MathWorks, Inc., Natick, MA). First, surfaces were registered rigidly, and then the templates were registered affinely to the periosteal bone surfaces. Subsequently, the articular cartilages were segmented. Intensity profiles were captured along surface normals for each vertex point at the bone–cartilage interface to determine the articular cartilage surface. Due to contrast enhancement, the joint space had high intensity whereas cartilage had low intensity; these local minima and maxima were used to determine the cartilage surface. A detailed explanation of the semi-automatic segmentation method was presented in a previous study [25].

Since the manual segmentation is widely regarded as the gold standard method [18,21,29], our models were compared against models generated by manual segmentation. Cartilages were segmented manually using Seg3D (v2.3, University of Utah, UT). Finally, all of the stereolithography (STL) surfaces were converted to a solid standard ACIS text format in MATLAB, and these geometries were meshed in Abaqus (v6.14, Dassault Systèmes, Providence, RI).

The surface mesh processing differed between semi-automatic and manual approaches and therefore the effect of the surface mesh processing was also examined. The surface meshes (STL) of semi-automatic segmentations were created directly from segmentations in MATLAB [25]. Additionally, the surfaces of semi-automatic segmentations were postprocessed similarly as those of the manual segmentations by using MIMICS with customized parameters (smoothness: 0.6, triangle reduction: 0.1). To analyze the effect of this specific postprocessing, the results from the FE models generated from these "modified semi-automatic" segmentations were compared with those generated from manual and semi-automatic segmentations.

Finite Element Meshes. Finite element meshes were created in ABAQUS (v6.14, Dassault Systèmes, Providence, RI) using first-order four-node porous continuum tetrahedral elements (type = C3D4P, one integration point in each element). The global distance between the nodes was set to 2 mm and 1 mm for the femoral and tibial cartilages, respectively, with a tolerance of 20% in size using both curvature control and minimum size control. Since the implemented loading caused high compressive strains, the stability of the meshes between the master (femoral cartilage) and slave (tibial cartilage) surfaces was ensured by doubling the density of the mesh of the slave surface. A sensitivity study was conducted using a mesh with six times the original element density (Fig. S1, which is available in the Supplemental Materials on the ASME Digital Collection).

Contact Definitions, Boundary Conditions, and Loading. To obtain sufficient contact interaction, the femoral cartilage was defined as a surface and the tibial cartilage was defined as a set of nodes. The discretization method between the master and slave surfaces was defined as a "surface-to-surface" contact with finite sliding; pressure-overclosure was evaluated as hard. Furthermore, tangential movements were defined as frictionless. Fluid flow was assumed to be negligible due to the application of high-rate dynamic loading [30] and hence free fluid flow was not allowed through the cartilage surfaces. The tibial bone–cartilage interface was fixed in all directions. The femoral bone–cartilage interface was coupled with a reference point, which was set in the middle-central between the medial and lateral epicondyles of the femur, similarly as in a previous study [7].

Instead of applying a simple axial loading, the simplified gait loading was applied in the models to enable a more extensive evaluation of the geometrical differences between the segmentation approaches. Similarly as in the earlier studies [7,31], joint motion and loading were run over 0.8 s, which covered one simplified stance phase. Movement determined in literature [32,33] was controlled using time-dependent boundary conditions. The force was scaled to match the weight of each subject by adjusting the maximum force to >2 times body weight. The flexion angle followed the simplified gait obtained from previous studies (Fig. 1(*c*)) [7,31]. Similarly as in those studies, a free varus-valgus

Table 1 Values of implemented material parameters for the fibril-reinforced poroviscoelastic (FRPVE) model

FRPVE material parameters [30]	Femoral cartilage	Tibial cartilage
E_m (MPa)	0.215	0.106
ν_m	0.15	0.15
E_0 (MPa)	0.92	0.18
E_ε (MPa)	150	23.06
η (MPa s)	1062	1062
k (10^{-15} $m^4N^{-1}s^{-1}$)	6	18
[a]n_f	0.8–0.15 h_z	0.8–0.15 h_z

Note: E_m = nonfibrillar matrix modulus, ν_m = Poisson's ratio of the nonfibrillar matrix, E_0 = initial fibril network modulus, E_ε = strain-dependent fibril network modulus, η = viscoelastic damping coefficient of fibrils, k = permeability, n_f = fluid fraction.
[a]Fluid distribution from the surface to the bone-cartilage interface where h_z indicates normalized depth (surface = 0, cartilage-bone interface = 1).

alignment was allowed to maintain sufficient tibiofemoral contact, i.e., constant contact at the medial and lateral compartments, during the introduced loading. Further motions were fixed: anterior–posterior and medial–lateral translations due to their subject-specific variation, and internal–external rotations due to their nonsystematic behavior between subjects [34,35]. This is a reasonable assumption, since the aim of this study was to compare the models generated by two different segmentation techniques.

Material Properties and Collagen Architecture. A previously validated fibril-reinforced poroviscoelastic (FRPVE) material model, which is able to capture tension-compression nonlinearity, was implemented for articular cartilage [36,37]. The total stress ($\boldsymbol{\sigma}_t$) of the material comprises the nonfibrillar matrix stress ($\boldsymbol{\sigma}_{nf}$), the fibril network stress ($\boldsymbol{\sigma}_f$), and the fluid pressure (p)

$$\boldsymbol{\sigma}_t = \boldsymbol{\sigma}_{nf} + \boldsymbol{\sigma}_f - p\mathbf{I} \tag{1}$$

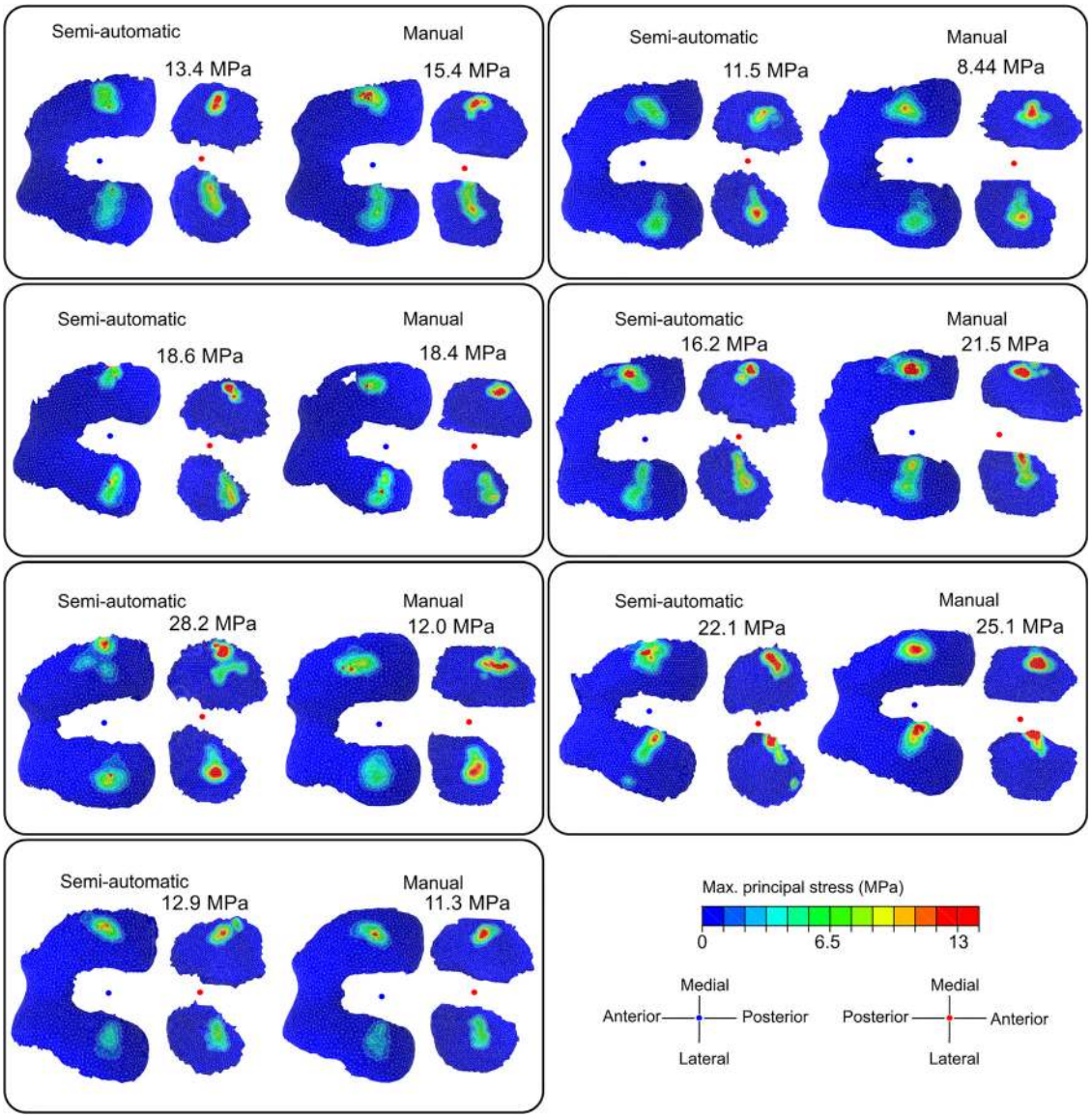

Fig. 2 Distribution of maximum principal stresses in the femoral and tibial condyle surfaces at 25% of the stance phase (first peak loading). The numerical values in the figure are the peak values of maximum principal stress (MPa) at the tibial surface. Colored dots indicate the corresponding anterior, posterior, medial, and lateral directions.

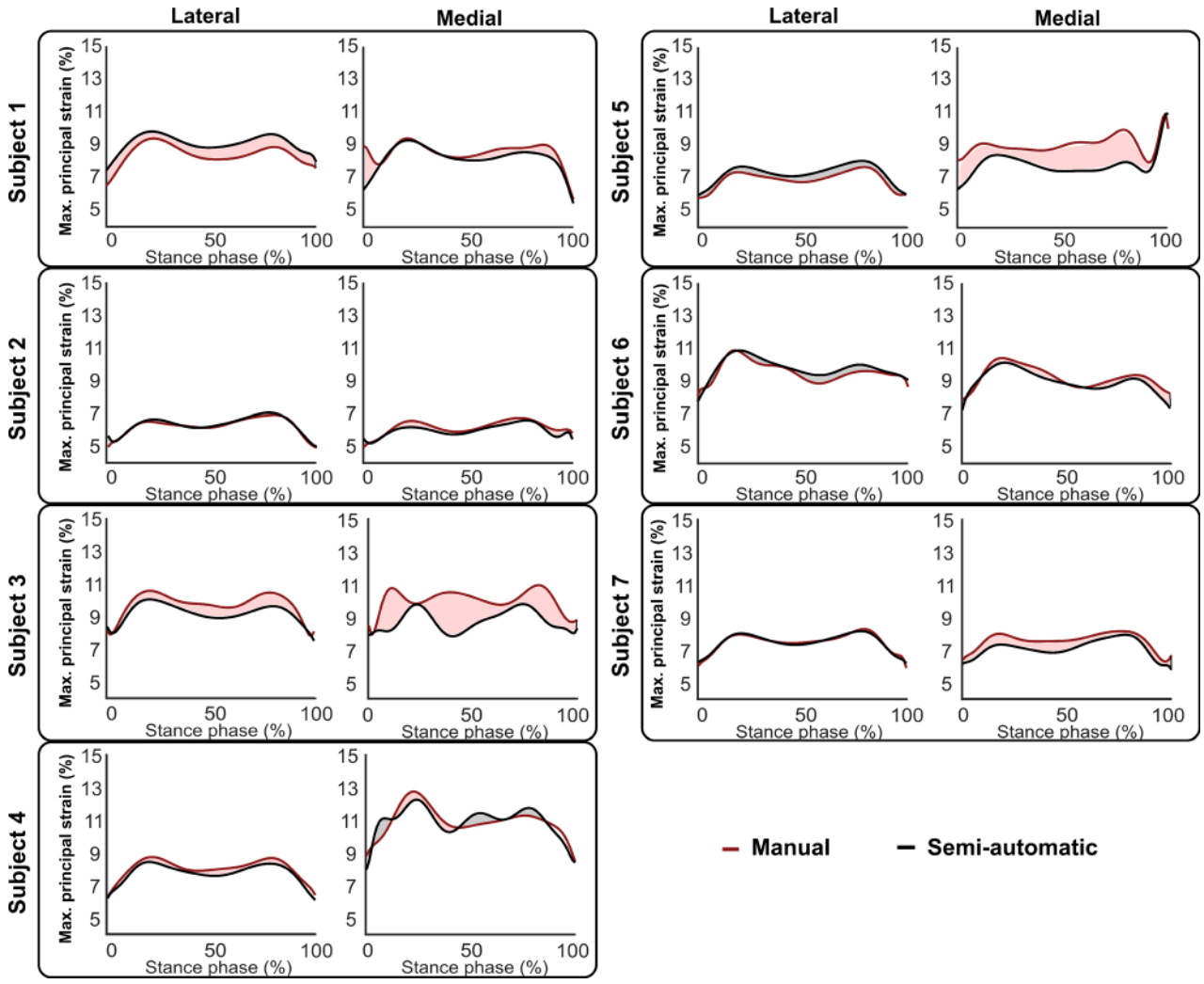

Fig. 3 Mean maximum principal strains (%) over the contact areas of the tibial compartments along the stance compared between the models generated from semi-automatic and manual segmentations of all the subjects

where **I** is the unit tensor. The chosen material parameters (Table 1) are based on an earlier experimental study [30]. The nonfibrillar matrix was modeled by the non-fibrillar matrix modulus (E_m) and Poisson's ratio (ν_m) using the neo-Hookean hyperelastic model, whereas the fibrillar network (17 fibrils in each integration point) was modeled by the viscoelastic primary and secondary fibrils with the initial fibril network modulus (E_0), strain-dependent fibril network modulus (E_ε) and viscoelastic damping coefficient (η). The effect of fluid support during dynamic loading was considered by Darcy's law using constant permeability (k) (see Supplemental Materials on the ASME Digital Collection for more details).

Based on previous studies [36–39], the primary collagen fibrils (four fibrils in each integration point) were oriented in specific split-line orientations, whereas the secondary fibrils (13 fibrils in each integration point) were randomly oriented. Fibril orientations for the secondary fibrils were coded directly in the user-defined material model (UMAT), model subroutine in ABAQUS, whereas the primary fibril orientations were first calculated in a global coordinate system separately for each integration point in each element using a custom MATLAB script and saved into a separate file. When solving models in ABAQUS, the primary fibril orientations were read by the UMAT subroutine. The definition for fibril implementation does not differ whether using hexahedral or tetrahedral meshes [15,40]. Since implementation of identical depth-dependent material properties of cartilage for each model would require identical tetrahedral element meshes, which was not the case between all compared models, depth dependency of the collagen fibril orientation was ignored. We wanted to ensure that differences between the models would be produced only by the geometry and not by the implementation of the fibril orientation. Thus, collagen fibrils were orientated parallel to the surface throughout the cartilage depth.

Simulations and Statistical Analysis. Model simulations were run implicitly with the ABAQUS/standard solver using consolidation analysis including three subsequent steps [31]. The first step included only an axial translation of femur to ensure an initial contact between the femoral and tibial cartilages (step duration = 0.1 s). The second step included an application of the initial force and flexion angle matching with the utilized data from the simplified gait loading (step duration = 0.1 s). The third step included a gait loading with time-dependent boundary conditions for the flexion angle and forces through the tibiofemoral joint (Fig. 1(*c*), step duration = 0.8 s).

Contact force and contact area of the tibiofemoral cartilage–cartilage contact were obtained from all the models. In addition, fibril strain, pore pressure, maximum principal strain (tensile strain), and maximum principal stress (tensile stress)

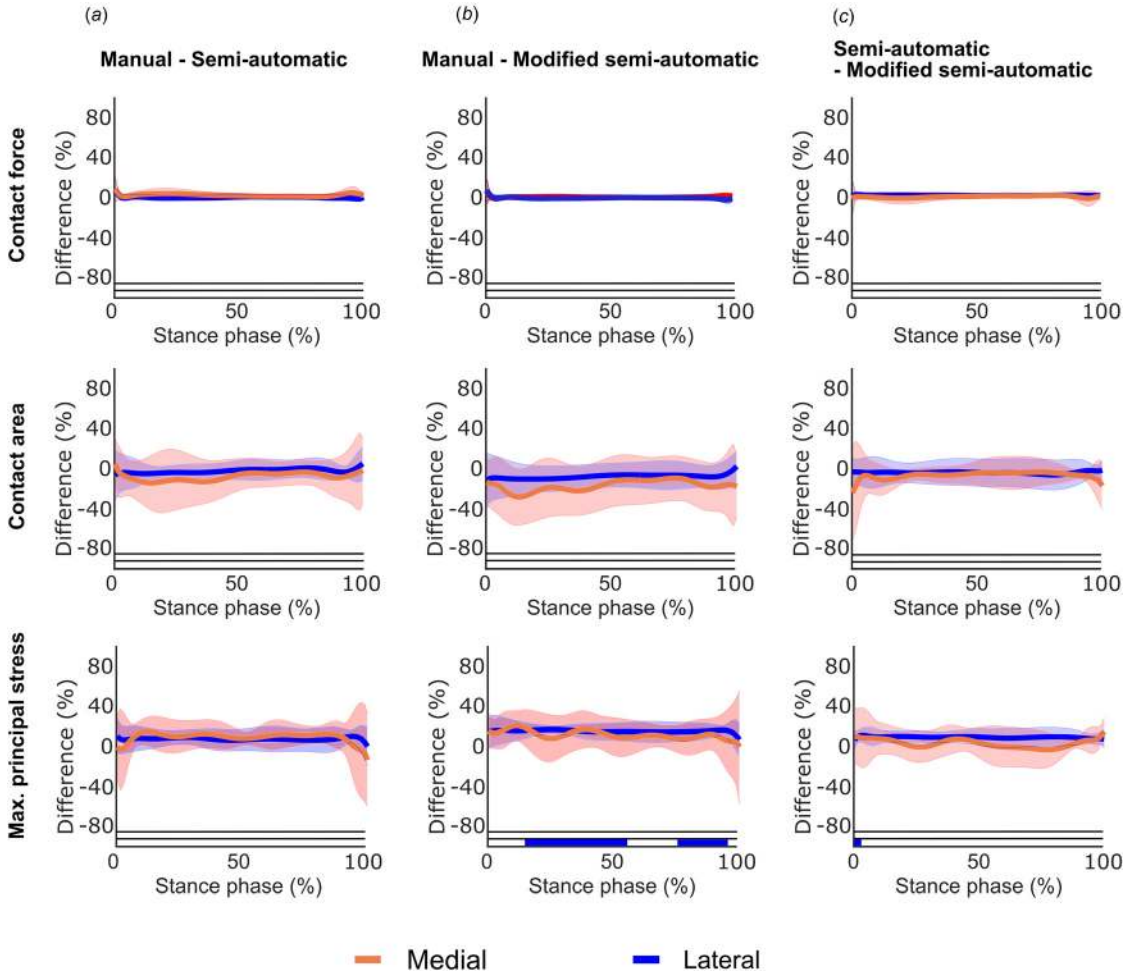

Fig. 4 Mean (line) and standard deviation (transparent color) of differences between the models generated by manual, semi-automatic, and modified semi-automatic segmentations; maximum principal stress, contact area, and contact force were compared in lateral and medial compartments of tibia. Colored lines at the bottom of each subgraph indicate statistical differences at each time point of the stance.

distributions were averaged over the tibiofemoral cartilage–cartilage contact area (Fig. 1(*c*)). All these parameters were then analyzed as a function of the stance.

The three models generated by manual and semi-automatic segmentation methods were compared against each other (manual versus semi-automatic; manual versus modified semi-automatic; semi-automatic versus modified semi-automatic). For each pair of the models, statistical differences of each parameter were examined over the stance phase by using 1D statistical parametric mapping implemented in MATLAB [41]. This method was chosen since the traditional methods, such as the parametric *t*-test or nonparametric Wilcoxon signed rank test, do not account for multiple comparisons on smooth and random 1D trajectories. Due to the low number of subjects, we used a nonparametric statistical parametric mapping approach that corresponds to the two-tailed dependent-samples Wilcoxon signed rank test. For comparison, we also conducted traditional Wilcoxon signed-rank tests (IBM® SPSS® Statistics, v21, IBM Corp., Armonk, NY) (see Supplemental Materials on the ASME Digital Collection).

Results

When the FE models based on manually and semi-automatically generated segmentations were compared at the first peak loading, i.e., at ∼25% of the stance phase, the distributions of maximum principal stresses were similar between the models for both the femoral and tibial cartilage surfaces (Fig. 2). Furthermore, neither of the models displayed systematically higher maximum stress values than the other; instead, the model with the highest stress values varied from subject to subject. (Fig. 2). Mean maximum principal strains on the contact area along the stance phase revealed only small and nonsystematic differences between the models (Fig. 3).

Differences in contact forces between the manual and semi-automatic FE models were minor, showing no systematic variation in the varus-valgus orientation (Fig. 4(*a*)). On the contrary, standard deviations (SDs) of contact area differences were relatively high. No statistically significant difference was found in the contact force or area between the models ($p \geq 0.05$). However, the maximum principal stress differed statistically significantly both in the medial and lateral compartments (Fig. 4(*a*)).

When the FE models generated from manual and semi-automatic segmentations were compared, pore pressure was the parameter, which exhibited the greatest variation (SD ∼11%). Nevertheless, the differences pore pressure values were statistically insignificant in both models ($p \geq 0.05$) (Fig. 5(*a*)). Differences were smallest in maximum principal strain and fibril strain. There were no significant differences in these parameters ($p \geq 0.05$) (Fig. 5(*a*)).

There was a better agreement when the values of fibril strain and maximum principal stress were obtained from the models generated by the manual and semi-automatic segmentations (Figs. 4(*a*) and 5(*a*)) as compared to the comparison of the models generated by the manual and modified semi-automatic

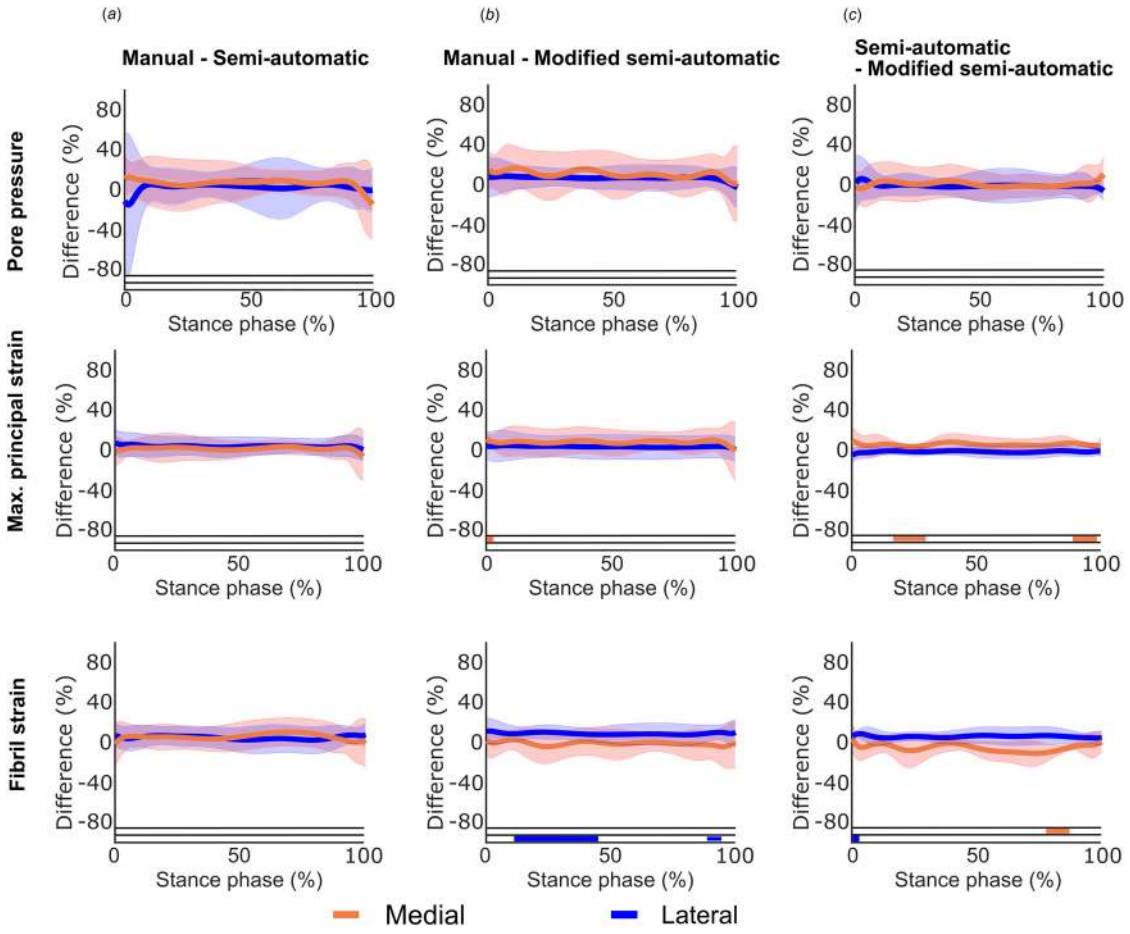

Fig. 5 Mean (line) and standard deviation (transparent color) of differences between the models generated from manual, semi-automatic, and modified semi-automatic segmentations; pore pressure, fibril strain, maximum principal strain were compared in lateral and medial compartments of tibia. Colored lines at the bottom of each subgraph indicate statistical differences at each time point of the stance.

segmentations (Figs. 4(*b*) and 5(*b*)). Moreover, statistical differences were detected between the models generated from semi-automatic and modified semi-automatic segmentations (Fig. 5(*c*)).

No systematic differences were observed in the parameters between the manual and semi-automatic approaches in a subject-wise manner (Fig. 6). These comparisons revealed that differences in the parameter values between the models were slightly higher in the medial compartment than in the lateral compartment. When comparing the models generated by the manual and semi-automatic segmentations, the mean absolute difference in the contact area was <25 mm^2 and <16 N in the contact force. The mean absolute differences in the maximum principal stress were <1 MPa and in the pore pressure <1.5 MPa. For the values of maximum principal strain and fibril strain, the mean absolute differences were $<0.72\%$ and $<0.40\%$, respectively.

The time required for manual segmentation of femoral cartilage was approximately 290 min and that of tibial cartilage was about 160 min. semi-automatic segmentation of femoral/tibial cartilage took approximately 20 min.

Discussion

In this study, we compared FE models generated from manually and semi-automatically segmented joint geometries of seven osteoarthritic knees. The semi-automated segmentation method enabled more rapid FE model generation while still achieving similar results as those obtained with the more time-consuming manual method.

There were only minor differences in maximum principal strain and fibril strain between the models generated from semi-automatic and manual segmentations. This suggests that cartilage strains may represent the most useful parameters that can be analyzed from FE models generated from semi-automatic segmentation. This would be advantageous in clinical practice since excessive tissue strains may be risk factors for cell death and proteoglycan loss [9,42,43]. Moreover, collagen fibril strains may be used in the prediction of collagen failure and the progression of fibril damage [10,11,44].

Another parameter, maximum principal stress, is often analyzed from FE models of the knee joint to reflect the point of cartilage failure [6,45,46] and the initiation and progression of OA [7,8]. In this study, even though maximum principal stresses showed more variation between the models when compared to strains, the mean difference in the absolute values of this parameter was less than 1 MPa. This small difference introduces very little uncertainty in the estimation of cartilage failure since cartilage failure stress in tension can vary from approximately $\sim$5 MPa to $\sim$15 MPa and is dependent on several factors, such as age, location, strain-rate, and OA grade of cartilage [7,15,47–50].

There has been a rapid development of automatic segmentation methods in the past few years. Neural networks, statistical shape models, and atlas-based methods provide a good basis for determining the geometries for soft tissues [19–23]. This study utilized a previously presented segmentation method [25] which reveals articular cartilage geometries; the method was proven to be accurate in terms of dice similarity coefficient, specificity, and

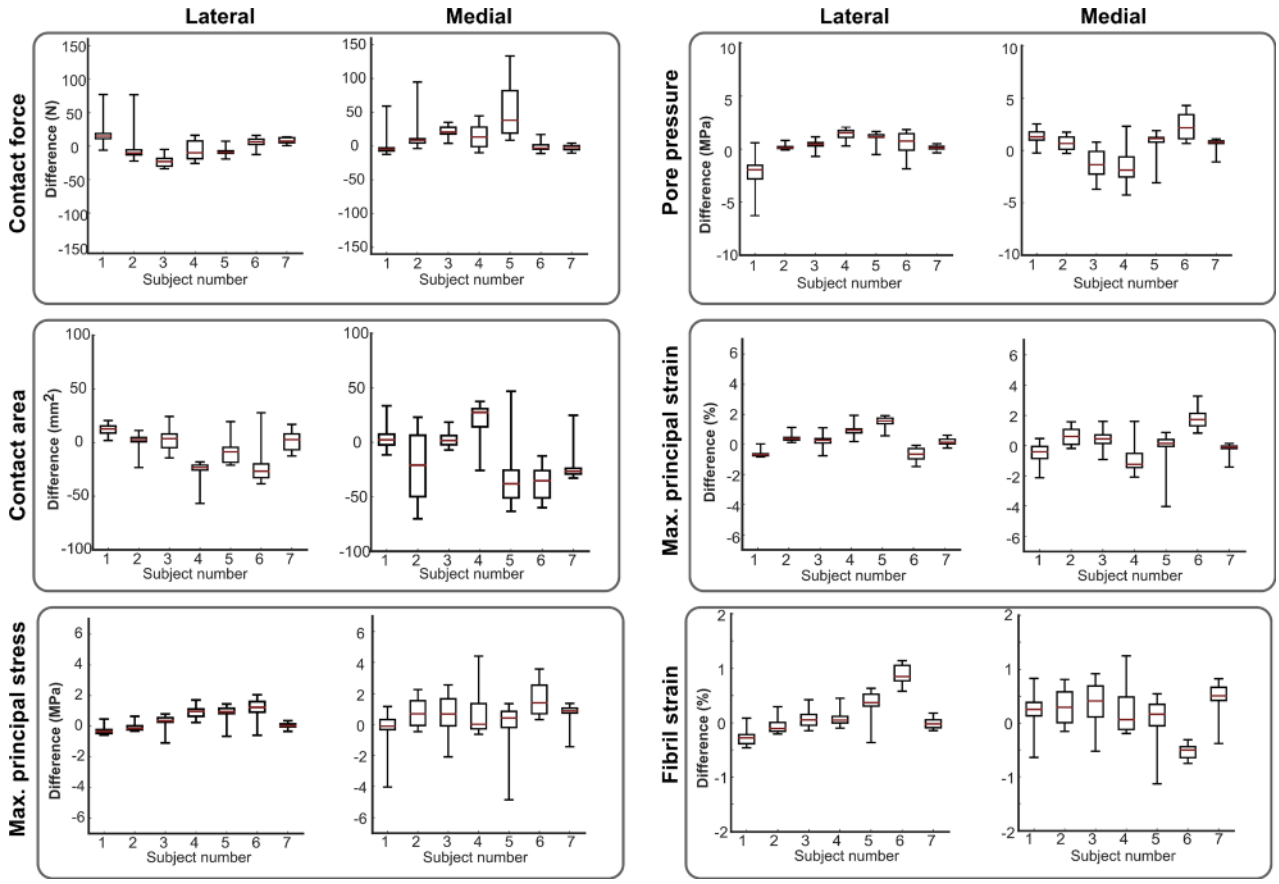

Fig. 6 The differences in contact area, contact force, maximum principal stress, maximum principal strain, pore pressure, and fibril strain calculated pairwise between the models generated from manual and semi-automatic segmentations (seven subjects)

sensitivity. The utilized technique has also been shown to enable an accurate determination of cortical bone thickness from CT images [28], which is beneficial when evaluating alterations related to OA. Importantly, articular cartilage surfaces were segmented automatically with the custom MATLAB script, leveraging the fact that administrated contrast agent provides a high degree of image contrast. Even though the segmentation method used in this study was not fully automatic, one important aspect was that the surfaces were generated in 3D. Most of the previously introduced segmentation methods rely on slice-by-slice 2D segmentations prior to the 3D construction of surfaces. Furthermore, the surfaces required no postprocessing for the presented modeling purposes.

Few semi-automatical segmentation methods have been combined with computational modeling [24,51]. These previously applied segmentation methods require modifications of the surfaces before they can be implemented into computational models. Furthermore, in these prior studies, simulations were conducted with a simple axial loading instead of applying more physiologically relevant loading conditions. Here, the segmented surface mesh of cartilage was directly used for both tetrahedral meshing and then applied in the subsequent steps in the modeling procedure. The semi-automatic segmentation approach to generate FE models described herein shows promise for analysis of joint function. However, mesh generation, assignment of boundary and loading conditions, and model analysis can be time-consuming, and require substantial domain expertise (i.e., expertise in computational biomechanics). Thus, future research should focus on automation of all steps of the FE modeling pipeline to support clinical application. For instance, automated or template-based FE meshing could also be included in the procedure [52].

In this study, the segmentation method was utilized for contrast-enhanced CT images. Since the pathological changes in OA occur in both bone and cartilage [53,54], contrast-enhanced CT can provide a comprehensive and quantitative analysis of these tissues as well as reveal detailed information on the topology of the cartilage surface. In future studies, the method could be tested for magnetic resonance images, which have been acquired with ultrafast spin-echo sequences that capture signal also from cortical bone.

Slight differences in cartilage topography, such as some roughness on the surface close to the edges, may explain the differences in the contact area and maximum principal stress between the models. For instance, even though the distributions of maximum principal stress were found to be similar (Fig. 2), some subjects displayed relatively high differences in the peak values. These differences may be reduced by improving the surface smoothing algorithm in the semi-automated segmentation method. However, when using the Mimics surface mesh generation, i.e., similar postprocessing of surfaces to that used in manual segmentations, to produce smoother surfaces (modified semi-automatic versus semi-automatic segmentation), the results were not really improved (Figs. 2 and 4). Instead, there were actually greater differences between the simulation results of the models generated from manual and modified semi-automatic segmentations. This again suggests usefulness of our segmentation method for biomechanical modeling purposes.

One limitation of this study is that the number of subjects was rather low which does not allow an extensive comparison of the models. Furthermore, since subject-specific gait information was unavailable, a simplified gait loading was implemented based on the literature [32]. Instead of having hexahedral meshes,

tetrahedral meshes were used since they were more suitable for assessing irregular segmented articular cartilage structures. The modeling results were also compared between the models with tetrahedral and hexahedral meshes and they were shown to be similar (Fig. S2 which is available in the Supplemental Materials on the ASME Digital Collection). Only articular cartilages were involved in the models since the present segmentation method is not suitable for handling other tissues, such as menisci. Nonetheless, the effect of menisci was evaluated, and it was observed that differences between the models remained the same whether or not menisci were included (Fig. S3 which is available in the Supplemental Materials on the ASME Digital Collection). Naturally, the lack of menisci influences the absolute values of the analyzed mechanical parameters, such as maximum principal stress. However, it was not necessary to include menisci herein since our primary objective was to compare cartilage mechanics predicted by the FE models generated using different segmentation techniques. Future research could focus on improving the semi-automatic segmentation algorithm to accommodate other soft tissues. Bones were considered as rigid in the models, which is a reasonable assumption, since bone is much stiffer than cartilage. Implementation of bones might slightly change cartilage responses [55]; however, it should not affect the conclusions of this study because the same rigid material assumption for bones was used in all of the models being compared against each other. The motion and forces through the tibiofemoral joint were generated using the known joint contact force and flexion angle of simplified gait [7,31], and, hence, it was not necessary to incorporate ligaments into these models [56].

In conclusion, a novel semi-automatic segmentation method was applied to generate geometries for FE modeling of cartilage biomechanics in the knee. The models generated from manual and semi-automatic segmentations produced similar results. However, semi-automatic segmentation was ten times faster. Thus, the semi-automatic segmentation method described and evaluated herein shows promise for future computational biomechanics studies of the knee and possible clinical application where the model geometry is generated from patient-specific CT arthrography scans.

Acknowledgment

The research leading to these results has received funding from the Academy of Finland (grant Nos. 286526, 305138, 269315, 324994, 328920, 324529, and 307932), the European Research Council (ERC) under the European Union's Horizon 2020 research and innovation programme (grant agreement No. 755037), Doctoral Program in Science, Technology, and Computing (SCITECO, University of Eastern Finland), The Research Committee of the Kuopio University Hospital Catchment Area for the State Research Funding (project 5041757) Kuopio, Finland, Sigrid Juselius Foundation, and Finnish Cultural Foundation. CSC—IT Center for Science, Finland, is acknowledged for providing computational resources and modelling software. Mimmi K. Liukkonen (Ph.D.) is acknowledged for the determination of meniscal supporting forces and Santtu Mikkonen (Ph.D.) is acknowledged for expertise in statistical analyses.

Funding Data

- Academy of Finland (Grant Nos. 286526, 305138, 269315, 324994, 328920, 324529, and 307932; Funder ID: 10.13039/501100002341).
- The European Research Council (ERC) under the European Union's Horizon 2020 research and innovation programme (Grant No. 755037; Funder ID: 10.13039/10001066).
- Doctoral Program in Science, Technology and Computing (SCITECO, University of Eastern Finland).
- The Research Committee of the Kuopio University Hospital Catchment Area for the State Research Funding (project 5041757) Kuopio, Finland (Funder ID: 10.13039/501100004092).
- Sigrid Juselius Foundation.
- Finnish Cultural Foundation.

References

[1] Cross, M., Smith, E., Hoy, D., Nolte, S., Ackerman, I., Fransen, M., Bridgett, L., Williams, S., Guillemin, F., Hill, C. L., Laslett, L. L., Jones, G., Cicuttini, F., Osborne, R., Vos, T., Buchbinder, R., Woolf, A., and March, L., 2014, "The Global Burden of Hip and Knee Osteoarthritis: Estimates From the Global Burden of Disease 2010 Study," Ann. Rheum. Dis., **73**(7), pp. 1323–1330.

[2] Christiansen, B. A., Anderson, M. J., Lee, C. A., Williams, J. C., Yik, J. H. N., and Haudenschild, D. R., 2012, "Musculoskeletal Changes Following Non-Invasive Knee Injury Using a Novel Mouse Model of Post-Traumatic Osteoarthritis," Osteoarthr. Cartil., **20**(7), pp. 773–782.

[3] Miller, R. H., Edwards, W. B., Brandon, S. C. E., Morton, A. M. Y. M., and Deluzio, K. J., 2014, "Why Don't Most Runners Get Knee Osteoarthritis? a Case for per-Unit-Distance Loads," Med. Sci. Sport. Exerc., **46**(3), pp. 572–579.

[4] Sadeghi, H., Shepherd, D. E. T., and Espino, D. M., 2015, "Effect of the Variation of Loading Frequency on Surface Failure of Bovine Articular Cartilage," Osteoarthr. Cartil., **23**(12), pp. 2252–2258.

[5] Azhar, A. A., Harris, M. D., Shalhoub, S., Maletsky, L. P., Rullkoetter, P. J., and Shelburne, K. B., 2018, "Combined Measurement and Modeling of Specimen-Specific Knee Mechanics for Healthy and ACL-Deficient Conditions," J. Biomech., **57**(24), pp. 117–124.

[6] Adouni, M., Shirazi-Adl, A., and Shirazi, R., 2012, "Computational Biodynamics of Human Knee Joint in Gait: From Muscle Forces to Cartilage Stresses," J. Biomech., **45**(12), pp. 2149–2156.

[7] Mononen, M. E., Tanska, P., Isaksson, H., and Korhonen, R. K., 2016, "A Novel Method to Simulate the Progression of Collagen Degeneration of Cartilage in the Knee: Data From the Osteoarthritis Initiative," Sci. Rep., **6**, p. 21415.

[8] Liukkonen, M. K., Mononen, M. E., Klets, O., Arokoski, J. P., Saarakkala, S., and Korhonen, R. K., 2017, "Simulation of Subject-Specific Progression of Knee Osteoarthritis and Comparison to Experimental Follow-Up Data: Data From the Osteoarthritis Initiative," Sci. Rep., **7**(1), p. 9177.

[9] Hosseini, S. M., Wilson, W., Ito, K., and van Donkelaar, C. C., 2014, "A Numerical Model to Study Mechanically Induced Initiation and Progression of Damage in Articular Cartilage," Osteoarthr. Cartil., **22**(1), pp. 95–103.

[10] Tanska, P., Julkunen, P., and Korhonen, R. K., 2018, "A Computational Algorithm to Simulate Disorganization of Collagen Network in Injured Articular Cartilage," Biomech. Model. Mechanobiol., **17**(3), pp. 689–699.

[11] Wilson, W., Huyghe, J. M., and van Donkelaar, C. C., 2006, "A Composition-Based Cartilage Model for the Assessment of Compositional Changes During Cartilage Damage and Adaptation," Osteoarthr. Cartil., **14**(6), pp. 554–560.

[12] Pierce, D. M., Ricken, T., and Holzapfel, G. A., 2013, "A Hyperelastic Biphasic Fibre-Reinforced Model of Articular Cartilage Considering Distributed Collagen Fibre Orientations: Continuum Basis, Computational Aspects and Applications," Comput. Methods Biomech. Biomed. Eng., **16**(12), pp. 1344–1361.

[13] Gu, K. B., and Li, L. P., 2011, "A Human Knee Joint Model Considering Fluid Pressure and Fiber Orientation in Cartilages and Menisci," Med. Eng. Phys., **33**(4), pp. 497–503.

[14] de Vries, S. A. H., van Turnhout, M. C., Oomens, C. W. J., Erdemir, A., Ito, K., and van Donkelaar, C. C., 2014, "Deformation Thresholds for Chondrocyte Death and the Protective Effect of the Pericellular Matrix," Tissue Eng. Part A, **20**(13–14), pp. 1870–1876.

[15] Venäläinen, M. S., Mononen, M. E., Salo, J., Räsänen, L. P., Jurvelin, J. S., Töyräs, J., Virén, T., and Korhonen, R. K., 2016, "Quantitative Evaluation of the Mechanical Risks Caused by Focal Cartilage Defects in the Knee," Sci. Rep., **6**, p. 37538.

[16] Lerner, Z. F., Damiano, D. L., and Bulea, T. C., 2019, "Computational Modeling of Neuromuscular Response to Swing-Phase Robotic Knee Extension Assistance in Cerebral Palsy," J. Biomech., **87**, pp. 142–149.

[17] Purevsuren, T., Khuyagbaatar, B., Kim, K., and Kim, Y. H., 2018, "Effects of Medial Collateral Ligament Release, Limb Correction, and Soft Tissue Laxity on Knee Joint Contact Force Distribution After Medial Opening Wedge High Tibial Osteotomy: A Computational Study," Comput. Methods Biomech. Biomed. Eng., **22**(3), pp. 243–250.

[18] Pedoia, V., Majumdar, S., and Link, T. M., 2016, "Segmentation of Joint and Musculoskeletal Tissue in the Study of Arthritis," Magn. Reson. Mater. Phys., **29**(2), pp. 207–221.

[19] Tabrizi, P. R., Zoroofi, R. A., Yokota, F., Nishii, T., and Sato, Y., 2016, "Shape-Based Acetabular Cartilage Segmentation: Application to CT AND MRI Datasets," Int. J. Comput. Assist. Radiol. Surg., 11(7), pp. 1–19.

[20] Pedoia, V., Li, X., Su, F., Calixto, N., and Majumdar, S., 2016, "Fully Automatic Analysis of the Knee Articular Cartilage T1p Relaxation Time Using Voxel-Based Relaxometry," J. Magn. Reson. Imaging, **43**(4), pp. 970–980.

[21] Fripp, J., Crozier, S., Warfield, S. K., and Ourselin, S., 2010, "Automatic Segmentation of Articular Cartilage in Magnetic Resonance Images of the Knee," IEEE Trans Med Imaging, **29**(1), pp. 55–64.

[22] Tamez-Peña, J. G., Farber, J., González, P. C., Schreyer, E., Schneider, E., and Totterman, S., 2012, "Unsupervised Segmentation and Quantification of

Anatomical Knee Features: Data From the Osteoarthritis Initiative," IEEE Trans. Biomed. Eng., **59**(4), pp. 1177–1186.
[23] Folkesson, J., Dam, E. B., Olsen, O. F., Pettersen, P. C., and Christiansen, C., 2007, "Segmenting Articular Cartilage Automatically Using a Voxel Classification Approach," IEEE Trans. Med. Imaging, **26**(1), pp. 106–115.
[24] Liukkonen, M. K., Mononen, M. E., Tanska, P., Saarakkala, S., Nieminen, M. T., and Korhonen, R. K., 2017, "Application of a Semi-Automatic Cartilage Segmentation Method for Biomechanical Modeling of the Knee Joint," Comput. Methods Biomech. Biomed. Eng., **20**(13), pp. 1453–1463.
[25] Myller, K. A. H., Honkanen, J. T. J., Jurvelin, J. S., Saarakkala, S., Töyräs, J., and Väänänen, S. P., 2018, "Method for Segmentation of Knee Articular Cartilages Based on Contrast-Enhanced CT Images," Ann. Biomed. Eng., **46**(11), pp. 1756–1767.
[26] Myller, K. A. H., Turunen, M. J., Honkanen, J. T. J., Väänänen, S. P., Iivarinen, J. T., Salo, J., Jurvelin, J. S., and Töyräs, J., 2017, "In Vivo Contrast-Enhanced Cone Beam CT Provides Quantitative Information on Articular Cartilage and Subchondral Bone," Ann. Biomed. Eng., **45**(3), pp. 811–818.
[27] Kokkonen, H. T., Suomalainen, J., Joukainen, A., Kröger, H., Sirola, J., Jurvelin, J., Salo, J., and Töyräs, J., 2014, "In Vivo Diagnostics of Human Knee Cartilage Lesions Using Delayed CBCT Arthrography," J. Orthop. Res., **32**(3), pp. 403–412.
[28] Treece, G. M. M., Gee, A. H. H., and Nigro, L., 2015, "Independent Measurement of Femoral Cortical Thickness and Cortical Bone Density Using Clinical CT," Med. Image Anal., **20**(1), pp. 249–264.
[29] Chu, C., Chen, C., Liu, L., and Zheng, G., 2015, "FACTS: Fully Automatic CT Segmentation of a Hip Joint," Ann. Biomed. Eng., **43**(5), pp. 1247–1259.
[30] Halonen, K. S., Mononen, M. E., Jurvelin, J. S., Töyräs, J., Salo, J., and Korhonen, R. K., 2014, "Deformation of Articular Cartilage During Static Loading of a Knee Joint—Experimental and Finite Element Analysis," J. Biomech., **47**(10), pp. 2467–2474.
[31] Mononen, M. E., Jurvelin, J. S., and Korhonen, R. K., 2015, "Implementation of a Gait Cycle Loading Into Healthy and Meniscectomised Knee Joint Models With Fibril-Reinforced Articular Cartilage," Comput. Methods Biomech. Biomed. Eng., **18**(2), pp. 141–152.
[32] Kutzner, I., Heinlein, B., Graichen, F., Bender, A., Rohlmann, A., Halder, A., Beier, A., and Bergmann, G., 2010, "Loading of the Knee Joint During Activities of Daily Living Measured In Vivo in Five Subjects," J. Biomech., **43**(11), pp. 2164–2173.
[33] Bergmann, G., Bender, A., Graich, F., Dymke, J., Rohlmann, A., Trepczynski, A., Heller, M. O., and Kutzner, I., 2014, "Standardized Loads Acting in Knee Implants," PLoS One, **9**(1), p. e86035.
[34] Kozanek, M., Hosseini, A., Liu, F., Van de Velde, S. K., Gill, T. J., Rubash, H. E., and Li, G., 2009, "Tibiofemoral Kinematics and Condylar Motion During the Stance Phase of Gait," J. Biomech., **42**(12), pp. 1877–1884.
[35] Li, J.-S., Tsai, T.-Y., Wang, S., Li, P., Kwon, Y.-M., Freiberg, A., Rubash, H. E., and Li, G., 2014, "Prediction of In Vivo Knee Joint Kinematics Using a Combined Dual Fluoroscopy Imaging and Statistical Shape Modeling Technique," ASME J. Biomech. Eng., **136**(12), p. 124503.
[36] Wilson, W., van Donkelaar, C. C., van Rietbergen, B., Ito, K., and Huiskes, R., 2004, "Stresses in the Local Collagen Network of Articular Cartilage: A Poroviscoelastic Fibril-Reinforced Finite Element Study," J. Biomech., **37**(3), pp. 357–366.
[37] Wilson, W., van Donkelaar, C. C., van Rietbergen, B., Ito, K., and Huiskes, R., 2005, "Erratum to 'Stresses in the Local Collagen Network of Articular Cartilage: A Poroviscoelastic Fibril-Reinforced Finite Element Study' [Journal of Biomechanics 37 (2004) 357–366] and "a Fibril-Reinforced Poroviscoelastic Swelling Model for Articular Cartil," J. Biomech., **38**(10), pp. 2138–2140.
[38] Goodwin, D. W., Wadghiri, Y. Z., Zhu, H., Vinton, C. J., Smith, E. D., and Dunn, J. F., 2004, "Macroscopic Structure of Articular Cartilage of the Tibial Plateau: Influence of a Characteristic Matrix Architecture on MRI Appearance," Am. J. Roentgenol., **182**(2), pp. 311–318.
[39] Benninghoff, A., 1925, "Form Und Bau Der Gelenkknorpel in Ihren Beziehungen Zur Funktion - Zweiter Teil: Der Aufbau Des Gelenkknorpels in Seinen Beziehungen Zur Funktion," Z. Für Zellforsch. Mikroskopische Anat., **2**(5), pp. 783–862.
[40] Mononen, M. E., Mikkola, M. T., Julkunen, P., Ojala, R., Nieminen, M. T., Jurvelin, J. S., and Korhonen, R. K., 2012, "Effect of Superficial Collagen Patterns and Fibrillation of Femoral Articular Cartilage on Knee Joint Mechanics-A 3D Finite Element Analysis," J. Biomech., **45**(3), pp. 579–587.
[41] Pataky, T. C., Vanrenterghem, J., and Robinson, M. A., 2015, "Zero- vs. One-Dimensional, Parametric vs. Non-Parametric, and Confidence Interval vs. Hypothesis Testing Procedures in One-Dimensional Biomechanical Trajectory Analysis," J. Biomech., **48**(7), pp. 1277–1285.
[42] Bartell, L. R., Fortier, L. A., Bonassar, L. J., and Cohen, I., 2015, "Measuring Microscale Strain Fields in Articular Cartilage During Rapid Impact Reveals Thresholds for Chondrocyte Death and a Protective Role for the Superficial Layer," J. Biomech., **48**(12), pp. 3440–3446.
[43] Párraga Quiroga, J. M., Wilson, W., Ito, K., and van Donkelaar, C. C., 2017, "The Effect of Loading Rate on the Development of Early Damage in Articular Cartilage," Biomech. Model. Mechanobiol., **16**(1), pp. 263–273.
[44] Stender, M. E., Regueiro, R. A., Klisch, S. M., and Ferguson, V. L., 2015, "An Equilibrium Constitutive Model of Anisotropic Cartilage Damage to Elucidate Mechanisms of Damage Initiation and Progression," ASME J. Biomech. Eng., **137**(8), pp. 81010–81013.
[45] Miramini, S., Smith, D. W., Zhang, L., and Gardiner, B. S., 2017, "The Spatio-Temporal Mechanical Environment of Healthy and Injured Human Cartilage During Sustained Activity and Its Role in Cartilage Damage," J. Mech. Behav. Biomed. Mater., **74**, pp. 1–10.
[46] Kiapour, A., Kiapour, A. M., Kaul, V., Quatman, C. E., Wordeman, S. C., Hewett, T. E., Demetropoulos, C. K., and Goel, V. K., 2013, "Finite Element Model of the Knee for Investigation of Injury Mechanisms: Development and Validation," ASME J. Biomech. Eng., **136**(1), p. 011002.
[47] Wilson, W., van Burken, C., van Donkelaar, C. C., Buma, P., van Rietbergen, B., and Huiskes, R., 2006, "Causes of Mechanically Induced Collagen Damage in Articular Cartilage," J. Orthop. Res., **24**(2), pp. 220–228.
[48] Tanska, P., Mononen, M. E., and Korhonen, R. K., 2015, "A Multi-Scale Finite Element Model for Investigation of Chondrocyte Mechanics in Normal and Medial Meniscectomy Human Knee Joint During Walking," J. Biomech., **48**(8), pp. 1397–1406.
[49] Kempson, G. E., 1982, "Relationship Between the Tensile Properties of Articular-Cartilage From the Human Knee and Age," Ann. Rheum. Dis., **41**(5), pp. 508–511.
[50] Sasazaki, Y., Shore, R., and Seedhom, B. B., 2006, "Deformation and Failure of Cartilage in the Tensile Mode," J. Anat., **208**(6), pp. 681–694.
[51] Baldwin, M. A., Langenderfer, J. E., Rullkoetter, P. J., and Laz, P. J., 2010, "Development of Subject-Specific and Statistical Shape Models of the Knee Using an Efficient Segmentation and Mesh-Morphing Approach," Comput. Methods Programs Biomed., **97**(3), pp. 232–240.
[52] Rodriguez-Vila, B., Sánchez-González, P., Oropesa, I., Gomez, E. J., and Pierce, D. M., 2017, "Automated Hexahedral Meshing of Knee Cartilage Structures–Application to Data from the Osteoarthritis Initiative," Computer Methods in Biomechanics and Biomedical Engineering, **20**(14), pp. 1543–1553.
[53] Burr, D. B., and Gallant, M. A., 2012, "Bone Remodelling in Osteoarthritis," Nat. Rev. Rheumatol., **8**(11), pp. 665–673.
[54] Goldring, S. R., 2009, "Role of Bone in Osteoarthritis Pathogenesis," Med. Clin. North Am., **93**(1), pp. 25–35.
[55] Venäläinen, M. S., Mononen, M. E., Väänänen, S. P., Jurvelin, J. S., Töyräs, J., Virén, T., and Korhonen, R. K., 2016, "Effect of Bone Inhomogeneity on Tibiofemoral Contact Mechanics During Physiological Loading," J. Biomech., **49**(7), pp. 1111–1120.
[56] Klets, O., Mononen, M. E., Tanska, P., Nieminen, M. T., Korhonen, R. K., and Saarakkala, S., 2016, "Comparison of Different Material Models of Articular Cartilage in 3D Computational Modeling of the Knee: Data From the Osteoarthritis Initiative (OAI)," J. Biomech., **49**(16), pp. 3891–3900.